Topological Insulator Nanowires Made by AFM Nanopatterning: Fabrication Process and Ultra Low-Temperature Transport Properties

Dmitry Yakovlev, Aleksei Frolov, Ivan Nazhestkin, Alexei Temiryazev, Andrey Orlov, Jonathan Shvartzberg, Sergey Dizhur, Vladimir Gurtovoi, Razmik Hovhannisyan, Vasily Stolyarov

ADVANCED PHYSICS RESEARCH
Open Access
www.advphysicsres.com

Topological Insulator Nanowires Made by AFM Nanopatterning: Fabrication Process and Ultra Low-Temperature Transport Properties

Dmitry S. Yakovlev, Aleksei V. Frolov, Ivan A. Nazhestkin, Alexei G. Temiryazev, Andrey P. Orlov, Jonathan Shvartzberg, Sergey E. Dizhur, Vladimir L. Gurtovoi, Razmik Hovhannisyan, and Vasily S. Stolyarov*

Topological insulator nanostructures became an essential platform for studying novel fundamental effects emerging at the nanoscale. However, conventional nanopatterning techniques, based on electron beam lithography and reactive ion etching of films, have inherent limitations of edge precision, resolution, and modification of surface properties, all of which are critical factors for topological insulator materials. In this study, an alternative approach for the fabrication of ultrathin Bi_2Se_3 nanoribbons is introduced by utilizing a diamond tip of an atomic force microscope (AFM) to cut atomically thin exfoliated films. This study includes an investigation of the magnetotransport properties of ultrathin Bi_2Se_3 topological insulator nanoribbons with controlled cross-sections at ultra-low 14 mK) temperatures. Current-dependent magnetoresistance oscillations are observed with the weak antilocalization effect, confirming the coherent propagation of 2D electrons around the nanoribbon surface's perimeter and the robustness of topologically protected surface states. In contrast to conventional lithography methods, this approach does not require a highly controlled clean room environment and can be executed under ambient conditions. Importantly, this method facilitates the precise patterning and can be applied to a wide range of 2D materials.

1. Introduction

The swift advancements in 2D materials research have been greatly facilitated by innovative nanofabrication methods. A variety of methods have been employed for creating nanostructures of conventional 3D topological insulators (TI) comprising Van der Waals bound binary compounds such as Bi_2Te_3,[1] Bi_2Se_3,[2–6] Sb_2Te_3,[7] and alloys of these elements. The fabrication of nanoribbons from these materials can be achieved through several techniques, including whisker growth or the nanostructuring of atomically thin films using electron beam lithography (EBL)[8] or focused ion beam (FIB) etching.[9,10] These films are typically produced via mechanical exfoliation, chemical vapor deposition (CVD), or molecular beam epitaxy (MBE). In-depth investigations of topologically protected surface states originated from studying the transport properties of

D. S. Yakovlev
Laboratoire de Physique et d'Etude des Matériaux, ESPCI Paris, CNRS
PSL University
Paris 75005, France
E-mail: dimitry.yakovlev@espci.fr

A. V. Frolov, A. P. Orlov
Kotel'nikov Institute of Radioengineering and Electronics of RAS
Mokhovaya str. 11-7, Moscow 125009, Russia

I. A. Nazhestkin, V. L. Gurtovoi
Russian Quantum Center
30 Bolshoi boul., Skolkovo 143025, Moscow Region, Russia

I. A. Nazhestkin, V. S. Stolyarov
Moscow Center for Advanced Studies
Kulakova str. 20, Moscow 123592, Russia

A. G. Temiryazev
Kotel'nikov Institute of Radioengineering and Electronics of RAS
Fryazino Branch
Vvedensky Sq. 1, Fryazino 141190, Moscow Region, Russia

A. P. Orlov
Institute of Nanotechnology of Microelectronics of RAS
Nagatinskaya str. 16A, Moscow 115487, Russia

J. Shvartzberg
Institute of Superconductivity and Institute of Nanotechnology
Department of Physics
Bar-Ilan University
Ramat-Gan 5290002, Israel

The ORCID identification number(s) for the author(s) of this article can be found under https://doi.org/10.1002/apxr.202400108

DOI: 10.1002/apxr.202400108

TI-nanoribbons which are fabricated by various methods.[11–16] Such nanostructures generally exhibit good transport properties, but the primary challenges include achieving precise control over the nanowire cross-section, adjusting the bulk carrier concentration, and avoiding surface oxidation. To address these challenges, a selective area approach using various thin film growth techniques can be employed. For instance, MBE-grown nanoribbons have a rectangular cross-section, making them scalable and suitable for Majorana surface, Solid-state and Gatemon architectures.[17–24] However, MBE requires a high-vacuum environment and precise control over the composition of the vapor used for growth, which can be challenging to achieve.[25–27] High-quality nanoribbons can also be fabricated using CVD[28,29] and physical vapor deposition (PVD)[30,31] methods, including the use of induction heaters.[32] Still, these methods risk sample contamination during the growth process. Standard methods like EBL and reactive ion etching (RIE)[33,34] for fabricating these structures sometimes fall short in edge homogeneity and resolution, particularly in applications such as quantum dots, nanowires, point contacts, and nanoribbons.[35–37] Alternative patterning methods are actively being developed to overcome these limitations and gain a deeper understanding of nanoscale phenomena.[38]

In this work, we employed a novel approach to fabricate Bi_2Se_3 nanoribbons using atomic force microscopy (AFM) pulse force nanolithography.[39,40] While the AFM probe is typically used for surface characterization of films and occasionally for the exfoliation of layered materials,[12,38,41] in our case, it serves a different purpose: to precisely cut thin films, locally generating an amorphous nonconducting region while operating in contact mode. The method involves point-by-point puncturing of an atomically thin exfoliated Bi_2Se_3 film with a diamond AFM tip, allowing the creation of nanoribbons with precise control over the width, length, and thickness. This technique enables the fabrication of ultrafine nanostructures on atomically thin films, facilitating diverse geometries[42] and topologies with exceptional precision, i.e., plasmon gratings.[43] Our method eliminates the need for vacuum operation and ensures that samples are free from contamination by polymer residues or substrate milling products. Moreover, AFM pulse force nanolithography provides a scalable and reproducible method for the fabrication of nanoribbons, which can be applied to complex multilayer heterostructures consisting of hBN,[44] graphene,[45] graphite,[46] $NbSe_2$,[47] WSe_2,[48] and high T_c laminates such as BSCCO.[49,50]

In our research, we evaluated the suitability of our fabrication method for TI nanostructures in topological quantum circuits. To do this, we focus on phase-coherent transport within a Bi_2Se_3 nanoribbon structure at an ultra-low temperature of 14 mK. We study the current-dependent universal conductance fluctuations (UCF) magnetoresistance oscillations. Recently, UCF oscillations have been intensively studied in quasi-2D topological insulators based on bismuth and antimony chalcogenides, like $Bi_{1.5}Sb_{0.5}Te_{1.8}Se_{1.2}$, $Bi_1Sb_1Te_{1.5}Se_{1.5}$, and $BiSbTe_3$ materials.[26,51–53] The results of these studies have provided insight into the electronic structure and topological properties of these materials.[52–54] We use multi-probe setups to examine how the ΔR_{UCF} varies with temperature and bias current I. This technique is a powerful tool for the thoroughly study of the properties inherent to high-mobility conducting states. Intriguingly, we observe the stability of these oscillation periods based on the applied bias current. The increasing current I considerably decreases the amplitude of the UCF oscillations. Our observations point toward the role of thermal excitation's energy-averaging effect and bias-induced energy dispersion in causing phase and coherence length decoherence.[55,56] Our attempts to use AFM pulse force nanolithography for TI systems shows promising results. Nevertheless, more information about the magnetotransport properties is needed for most stoichiometries. Further studies in this area will likely reveal new and exciting results regarding the basic physics of these materials.

2. Results

Figure 1a presents a schematic illustration of the sample fabrication process. To briefly summarize the method, we initially employed an AFM with diamond tip cantilevers[57] to perform mechanical patterning of single crystalline Bi_2Se_3 flakes exfoliated at SiO_2 substrate covered with thin epoxy layer. The process of film exfoliation as well, as AFM lithography and contact preparation is described in detail in the Experimental Section. The AFM image of the fabricated nanoribbon is shown in Figure 1b. The technique combining optical, atomic force, and scanning electron microscopy allowed us to control the width of the nanoribbon within 10 nm (Figure 1c, SEM-image) and the thickness of the film with an accuracy of one quintuple layer Se-Bi-Se-Bi-Se (QL), which is ≈1 nm thick. Also, the advantage of our fabrication technique and measurement setup was the ability to produce several nanowires on segments of varying thickness from the same film, all oriented in the same direction, Figure 1c,d. In particular, the sample on which the main results of the work were obtained consisted of six nanowires (Samples *#A-#F*), connected in series, three of which are shown in Figure 1c. This configuration enables multi-probe electron transport measurements within a single cryostat cooldown cycle, all under the same magnetic field direction. The microscope image of the fabricated sample with measurement probes are shown in Supporting Information, Figure S1. The parameters of nanowires are shown in **Table 1**. The resistances of the Bi_2Se_3 junctions ranged from 5 to 45 kΩ at room temperature. Due to their high length-to-width ratio, the nanowires exhibit much higher resistance compared to the contacts and the connecting film segments.

S. E. Dizhur
Department of Condensed Matter Physics
Weizmann Institute of Science
Herzl Street, Rehovot 76100, Israel
R. Hovhannisyan
Department of Physics
Stockholm University, AlbaNova University Center, Universitetsvägen
Stockholm SE-10691, Sweden
V. S. Stolyarov
Laboratoire de Physique et d'Etude des Matériaux, ESPCI-Paris
PSL University
Paris 75005, France
V. S. Stolyarov
National University of Science and Technology MISIS
4 Leninsky Avenue, Moscow 119049, Russia

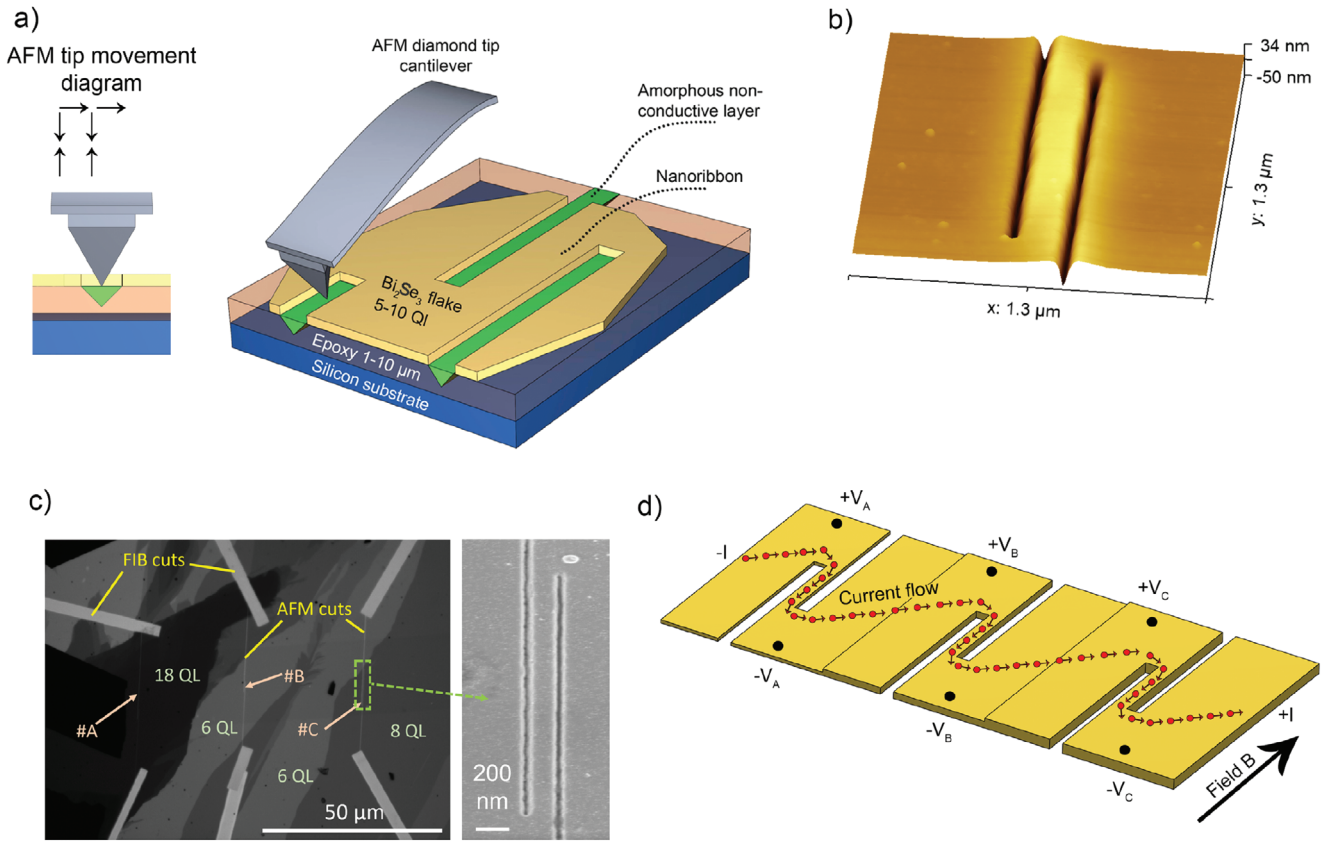

Figure 1. Nanoribbon of topological insulators: fabrication process a) Schematic illustration of nanoribbon fabrication from atomically thin Bi_2Se_3 film using AFM tip cutting. The tip sequentially pierces the film with a 5–10 nm step in the *y* direction, thus creating a cut. The inset on the left provides a cross-sectional view and a motion diagram of the AFM tip. b) Atomic force microscope 3D profile of nanoribbon after fabrication. c) Image of nanoribbons #A, #B, and #C in optical microscope in transmission regimes accompanied by a scanning electron microscope (SEM) image of the nanoribbon #C. Nanoribbons are fabricated within the FIB-made cuts. The thicknesses of some chosen areas are pointed out. d) The layout of current propagation through Bi_2Se_3 nanowires during magnetotransport measurements: current flows through the entire device, and voltage is measured across different segments.

The experimental configuration, illustrated in Figure S2 (Supporting Information), involved applying a symmetric bias to the sample using a current derived from a voltage source, a symmetrizing circuit, and a precise resistor. The swept current and the resulting voltage were then amplified through instrumentation amplifiers and captured using a 24-bit analog-to-digital converter (ADC). For more specific details regarding the measurements, please refer to the Methods section.

Table 1. Overview of the geometry of the five different nanoribbon devices investigated.

Sample	$R_{14mK,\ 3nA}$, kΩ	Ql	Length, μm	Width, nm	$\rho_{14mK,\ 3nA}$, μΩ · m	Cut Nº.
A	3.6	18	3	210	4.5	4
B	18.5	6	3	210	6.9	3
C	35.1	8	10	210	5.8	2
D	13.0	8	3	210	6.9	1
E	12.4	9	3	210	6.6	5
F	10.3	8	3	210	6.5	6

All nanoribbons exhibited metallic behavior ($dR/dT > 0$) from 300 K down to 2 K, with the resistances of these samples decreasing almost linearly due to electron–phonon scattering of the bulk carriers. However, below 2 K, a significant behavior change was observed, with the resistance of one junction showing a 700 Ω kink (Figure S3, Supporting Information). This resistance kink is believed to be due to manifestations of surface-state resistance against the background of bulk carriers freezing in topological insulators. It is more prominent in thinner samples.[27,58,59]

Figure 2a,b shows the experimentally obtained magnetoresistance of four nanowires of different sizes with a magnetic field applied parallel to the nanoribbon axis. Continuous field sweeps from –6 to 6 T were performed with various applied bias currents. First, a sharp increase in magnetoresistance is observed in the magnetic field range of $|H|$ <0.5 T, due to weak antilocalization (WAL) in Bi_2Se_3 resulting from strong spin-orbit interaction. Second, at higher magnetic field values ($|H| > 0.5$ T), conductance oscillations are observed. Both the WAL effect and magnetoresistance oscillations arise from the interference of topological surface states. In a magnetic field parallel to the axis of the nanowire, one can expect periodic Aharonov–Bohm and Altshuler–Aronov–Spivak oscillations with periods $\Phi_0 = hc/e$

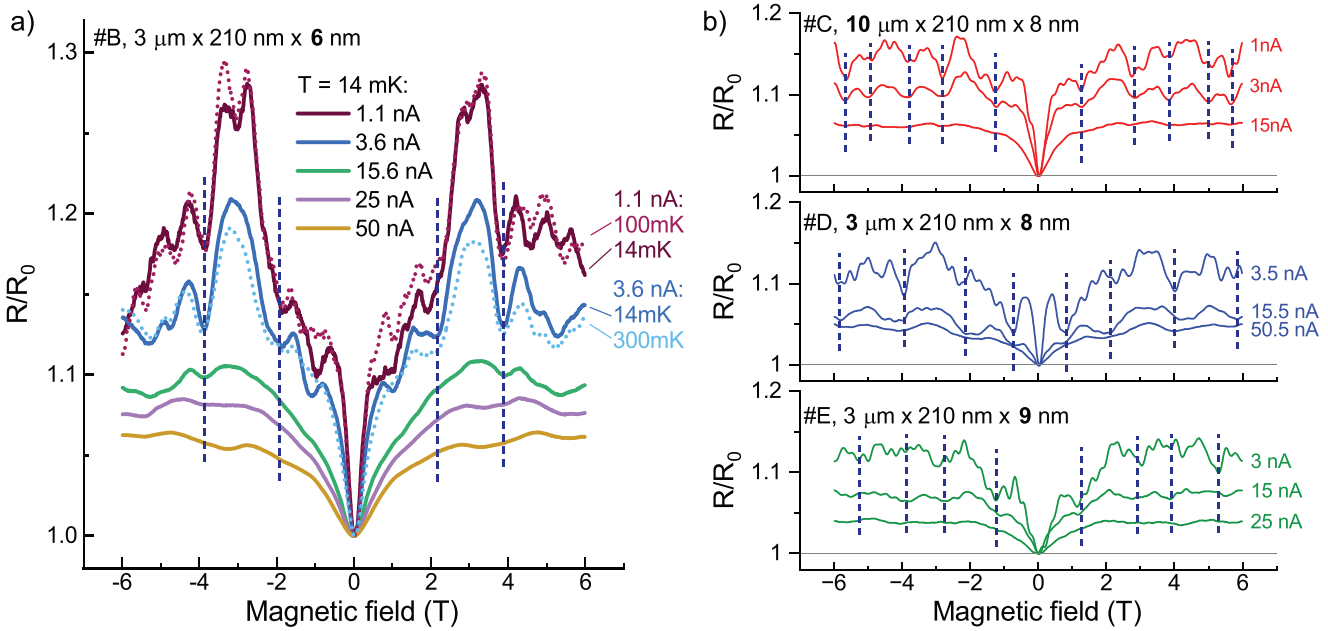

Figure 2. Bi_2Se_3 nanoribbons: magnetic field measurements at various currents. a,b) Normalized magnetoresistance of nanoribbons versus longitudinal magnetic field at different bias currents at 14 mK. A distinct modulation of the resistance (dashed lines) is observed, with a period close to threading of one flux quantum (hc/e) into the cross-section of the nanoribbon. For nanoribbon #*B*, R_0 = 18.9 kΩ, for #*C* R_0 = 34.8 kΩ; for #*D*, R_0 = 12.6 kΩ; for #*E*, R_0 = 12.4 kΩ.

and $\Phi_0/2 = hc/2e$ where Φ_0 is a flux quantum through the cross-section of the nanowire. Since all the nanowires under study have the same width, the period of magnetic field oscillations is inversely proportional to their thickness, varying from 2.2 T at t = 9 nm to 3.3 T at t = 6 nm. The period of oscillations, marked with dashed lines in Figure 2a,b, is closer to $\Phi_0/2 = hc/2e$, but the oscillation structure is not fully periodic. Moreover, the structure of oscillations in nanowires #C and #D, which have the same cross-section, differs significantly. This suggests that we are observing universal conductance fluctuations. At low currents, more minor period oscillations ≈0.5 T are observed, but they are non-reproducible for various field sweep directions (Figure S4, Supporting Information) and are attributed to noise-like fluctuations.

One notable effect we observe is that the amplitude of oscillations, attributed to UCF, decreases significantly with increasing current. This is observed for all the measured samples and can be associated with the reduction in the phase-coherence length.[60,61] Typically, the damping of universal conductance fluctuations is observed with an increase in temperature.[51–53] In our case, both increasing temperature and current reduce the oscillation amplitude. However, the influence of current is more significant at low temperatures. Indeed, in the millikelvin temperature range, heat exchange between the nanowire and the environment can become extremely limited, causing significant local overheating even at nanoampere currents. In the Supporting Information, we considered the main heat paths (Table S1, Supporting Information) and estimated that the maximum temperature gradient between the middle of the nanowire and the mixing chamber flange of our dilution cryostat (T_{mix} = 14 mK) does not exceed 0.75 mK at currents below = 5 nA. Figure 2a supports our estimation: showing visible temperature damping of oscillations only at T_{mix} = 300 mK, while current damping is very strong when changing the current from 1.1 to 3.6 nA.

To study the dephasing rate in our samples and the current dependence of the UCF amplitude, we focus on the current range above 1 nA. The empirical relation for the temperature dependence of ΔR_{UCF} is

$$\Delta R_{UCF} = \alpha exp(-\beta I) \quad (1)$$

where α and β are the fitting parameters. The dashed blue lines shown in Figure S5b (Supporting Information) are fitted with the equation above. The dephasing rate can be extracted from the parameter β. For all measurements, the values of β are around 0.3. Previous studies have shown that the specific dephasing source is the voltage and temperature fluctuations.[62,63] In our case, current-induced dephasing is a process that originated in the thermal averaging effect. Notably, the current dependence of R_{UCF} is also insensitive to probe configuration as shown in Figure 2b.

The magnetoresistance feature near zero field sourced from the weak antilocalization effect as was described by the Hikami–Larkin–Nagaoka (HLN) theory. In brief, the conductance field dependence near the zero field can be expressed as follows:

$$G(B) = G_0 - \alpha \frac{e^2}{2\pi^2\hbar}\left(\Psi\left(\frac{1}{2} + \frac{\hbar}{4eL_\phi^2 B}\right) - \ln\left(\frac{\hbar}{4eL_\phi^2 B}\right)\right) \quad (2)$$

where α is related to the number of channels carrying the π Berry phase or providing the strong spin-orbit coupling (0.5 for each channel), L_ϕ is the electron phase coherence length (the distance traveled by the electron before its phase is changed), and Ψ is the digamma function.[64,65] The parameters α and L_ϕ

Table 2. Fit parameters for Hikami–Larkin–Nagaoka (HLN) theory describing the weak antilocalization effect in different nanoribbon devices measured at the bias current I_b=30 nA.

Nanoribbon	Current, nA	L_ϕ, nm	α
B	0.3 nA	172.80 ± 9.44	0.47 ± 0.03
C	15 nA	61.85 ± 2.58	0.09 ± 0.01
E	15 nA	118.73 ± 6.40	0.15 ± 0.01

were determined with the fit and are shown in **Table 2**. The fit results for different nanoribbons are shown in **Figure 3**a,c,d. A theoretical function provides a good explanation for the antilocalization feature on magnetoresistance curves. Phase coherence length L_ϕ is consistent in order of magnitude with earlier results for Bi_2Se_3.[27,66,67] The relatively small values $\alpha \sim 0.5$ (at smallest bias currents) are the marker of dominating of surface states contribution and minor contribution of bulk states.[68] Understanding the exact nature of such transport, of the ratio between surface and bulk state contributions requires further investigation. Figure 3b shows the dependence of phase coherence length L_ϕ and parameter α on the bias current at which the oscillations were measured. They exhibit slight decrement with the increased bias current. Some discrepancies from the monotonic behavior can be explained by the imprecise current setting for small currents (in order of nA), but the trend to decrease is visible. The dephasing field $B_\phi = \hbar/4eL_\phi^2$[69] increases with increasing current, which reconfirms the current-induced dephasing mechanism. The channel number constant α also decreases with bias current, which increases channel separation with current. In previous works, a similar effect was caused by increased temperature,[70] consistent with our proposal of the same effect of temperature and current.

3. Conclusion

In conclusion, we have demonstrated a novel approach for the fabrication of topological insulator nanoribbons with precise ge-

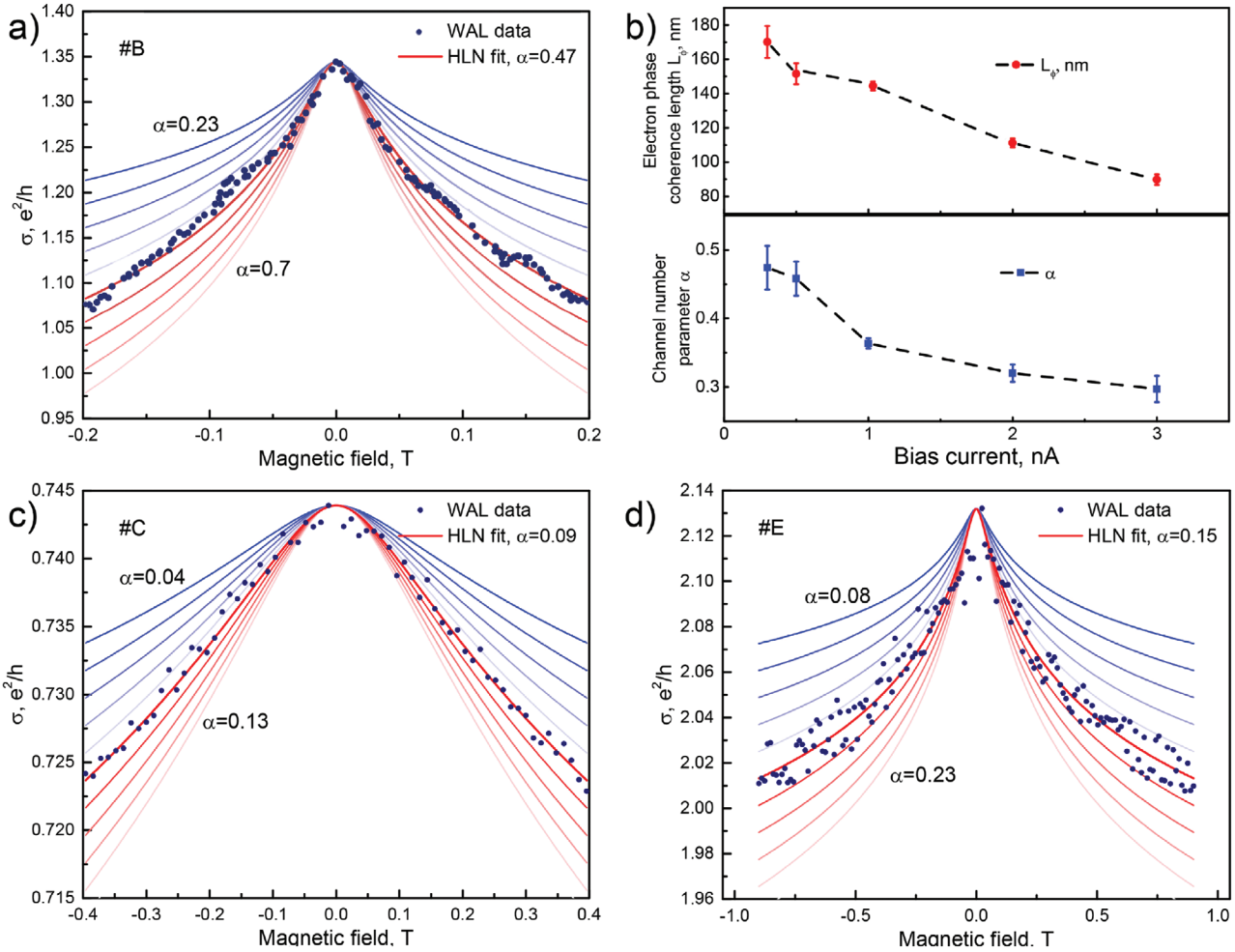

Figure 3. Weak antilocalization behavior of three nanoribbons with different thicknesses in QL units fitted with the Hikami–Larkin–Nagaoka (HLN) model. a) Nanoribbon B (length 3 μm, 6 QL), measured at bias current I_b = 0.3 nA. b) Actual fit parameters: electron phase coherence length L_ϕ and channel parameter α for nanoribbon B for different bias currents. c) Nanoribbon C (length 10 μm, 6 QL), measured at bias current I_b = 15 nA. d) sample E (length 3 μm, 8 QL), measured at bias current I_b = 15 nA. The fit with the HLN theory is shown with red solid lines. HLN curves obtained by variation of the channel number parameter α at fixed optimal L_ϕ obtained from fitting is shown by solid lines of different color.

ometric control, achieved through the nanopatterning of atomically thin exfoliated films using a diamond tip of an atomic force microscope (AFM). The Bi_2Se_3 nanoribbons studied at ultra-low (14 mK) temperatures revealed the emergence of magnetoresistance oscillations and a weak antilocalization effect with a remarkable dependence on the applied current. These results driven by the behavior of topologically protected states not only validate the high quality of the fabricated structures but also highlight the potential of the AFM-based nanopatterning method for fine-tuning of nanoribbon geometry thus allowing the study of thickness dependence and layer-by-layer evolution of topological properties.

4. Experimental Section

Sample Preparation: Bi_2Se_3 films were fabricated from bulk crystals grown using the standard Bridgman technique described elsewhere.[71] The typical carrier concentration of bulk samples was $10^{19} cm^{-3}$. Fragments of the initial bulk crystal with clean, flat surface were fixed to a sapphire substrate using a two-component epoxy adhesive. These fragments were then to nanometer thickness by successive exfoliation with adhesive tape.[72] Typically, this process yields a continuous film of approximately 1 × 1 mm, containing areas of uniform thickness with lateral dimensions of 10–200 microns and thicknesses of 1–100 quintuple layers. The thickness of the Bi_2Se_3 film was estimated by: a) the transparency of the films after exfoliation; b) by AFM scanning before and after pulse force nanolithography; c) scanning electron microscopy after all measurements. Electrical contacts were made immediately after exfoliation by cold indium soldering directly to the film. Based on the position of the contacts, 20 μm wide jumpers were fabricated using mechanical methods and laser ablation. The narrowest parts of the jumpers, barely visible in optical microscope (Figure 2a), were structured by focused ion beam (FIB) milling. Nanoribbons were subsequently produced by creating two parallel cuts using AFM indentation nanolithography under ambient conditions with a commercial atomic force microscope (SmartSPM, AIST-NT) and a silicon cantilever with a single crystal diamond tip.[57,73] To avoid sample surface degradation, the film's exposure was minimized to the atmosphere after exfoliation by using desiccators and masking the main areas of the film before cutting with the FIB.

Measurement details: The DC measurements were performed in a BlueFors LD-250 dilution refrigerator equipped with a copper sample holder that is carefully shielded against electromagnetic interference with a mu-metal shield. Four-contact measurements were employed with separate BeCu/NbTi twisted pairs for the current and voltage contacts of the structures. To minimize the switching noise from the inputs of the analog-to-digital conversion (ADC) card, the Leonardo II ADC card measures signals from the outputs of current and voltage instrumentation amplifiers (IAs) (AD8220 and AD8421, respectively), as shown in Figure 1d, rather than directly from the samples. Amplifiers increase the millivolt signal into the volt range to be registered with an ADC. To improve the accuracy of the current signal, it was additionally corrected, and an inverted voltage drop on the sample was considered (used as a reference for the AD8220 amplifier). All 12V amplifier power lines were equipped with 1 μF capacitors to decouple the power lines from noise and signal generated in the device. All electrical inputs and outputs of the cryostat are filtered by pi-filters (C = 2.5 nF), followed by a two-stage symmetric low-pass RC-filter based on surface-mounted lumped elements (R = 1 kΩ, C = 100 nF, with a cut-off frequency of 1.7 kHz) at the 4K-flange. Finally, a compact distributed RC silver-epoxy microwave filter made of twelve 1.6-meter-long twisted pairs (TP-filter) was used, which is located at the input to the sample holder on the Mixing Chamber flange. To verify its microwave operation, a specially designed 1-meter-long silver-epoxy filter with SMA connectors was tested, demonstrating more than 100 dB attenuation in the frequency range of 0.1–20 GHz. This is in accordance with the estimations, which suggest that the 1.6-meter TP-filter should result in more than 150 dB attenuation in the same frequency range. The same experimental setup was employed to measure various types of magnetic field oscillations at low temperatures.[74,75].

The room temperature voltage amplification was performed by a homemade symmetric amplifier system with a voltage noise density of 3 nV $Hz^{-1/2}$ and symmetric current biasing of samples by a voltage symmetrizer. The symmetrizer, based on the instrumentation amplifier LT1167, receives a differential output from a voltage source, while an operational amplifier OP177 operates in inverter mode and provides an opposing current. The source of voltage biasing to the voltage symmetrizer is an ultra-low distortion function generator DS360. The amplifier is mounted in an aluminum box to provide electromagnetic shielding. The symmetry of the amplifiers, the biasing, and DC twisted pairs results in solid suppression of standard mode low-frequency interference (50 Hz and harmonics). Two of the eight synchronous channels of the 24-bit ADC card digitize calibrated voltage and current signals at a rate of 102.4 kHz. This data, along with Lakeshore bridge measured temperature data, is written to files according to algorithms of proper DC measurements (V(I), Ic(B), Ic(T), R(T)).

Supporting Information

Supporting Information is available from the Wiley Online Library or from the author.

Acknowledgements

The work of I.A.N. and V.L.G. was supported by The framework of the Roadmap for Quantum computing (Contract No. 868-1.3-15/15-2021 dated October 5). The work of D.S.Y. was supported by ANR JCJC (HECTOR 308 ANR-21-CE47-0002-01) and by Thales and Airbus through a Cofund fellowship. The research at ultra-low temperatures was carried out with the support of a Grant from the Ministry of Science and Higher Education No. 075-15-2024-632 from June 14, 2024.

Conflict of Interest

The authors declare no conflict of interest.

Author Contributions

V.S.S. and A.V.F. conceived the experiment. A.V.F., A.G.T., A.P.O., and S.D. fabricated the samples. D.S.Y., V.L.G., and I.A.N. performed the experiments. D.S.Y., A.V.F., I.A.N., R.H., and J.S. analyzed the data. D.S.Y., I.A.N., and A.V.F. wrote the manuscript with input from all authors. All authors discussed the results and their implications equally.

Data Availability Statement

The data that support the findings of this study are available from the corresponding author upon reasonable request.

Keywords

AFM cutting, magneto-resistance oscillations, pulse force nanolithography, topological insulator, UCF, ultra-low temperature

Received: July 20, 2024
Revised: September 7, 2024
Published online:

[1] X. Zhang, X. Liu, C. Zhang, S. Peng, H. Zhou, L. He, J. Gou, X. Wang, J. Wang, *ACS Nano* **2022**, *16*, 4851.
[2] H.-S. Kim, T.-H. Hwang, N.-H. Kim, Y. Hou, D. Yu, H.-S. Sim, Y.-J. Doh, *ACS Nano* **2020**, *14*, 14118.
[3] A. Assouline, C. Feuillet-Palma, N. Bergeal, T. Zhang, A. Mottaghizadeh, A. Zimmers, E. Lhuillier, M. Eddrie, P. Atkinson, M. Aprili, H. Aubin, *Nat. Commun.* **2019**, *10*, 126.
[4] V. Stolyarov, S. Remizov, D. Shapiro, S. Pons, S. Vlaic, H. Aubin, D. Baranov, C. Brun, L. Yashina, S. Bozhko, T. Cren, W. V. Pogosov, D. Roditchev, *Appl. Phys. Lett.* **2017**, *111*, 25.
[5] V. S. Stolyarov, D. S. Yakovlev, S. N. Kozlov, O. V. Skryabina, D. S. Lvov, A. I. Gumarov, O. V. Emelyanova, P. S. Dzhumaev, I. V. Shchetinin, R. A. Hovhannisyan, S. V. Egorov, A. M. Kokotin, W. V. Pogosov, V. V. Ryazanov, M. Y. Kupriyanov, A. A. Golubov, D. Roditchev, *Commun. Mater.* **2020**, *1*, 38.
[6] V. Stolyarov, S. Kozlov, D. Yakovlev, N. Bergeal, C. Feuillet-Palma, D. Lvov, O. Skryabina, M. Kupriyanov, A. Golubov, D. Roditchev, *arXiv preprint arXiv:2309.10897* **2023**.
[7] L. Locatelli, A. Kumar, P. Tsipas, A. Dimoulas, E. Longo, R. Mantovan, *Sci. Rep.* **2022**, *12*, 3891.
[8] S. Cho, B. Dellabetta, R. Zhong, J. Schneeloch, T. Liu, G. Gu, M. J. Gilbert, N. Mason, *Nat. Commun.* **2015**, *6*, 7634.
[9] B. Bhattacharyya, A. Sharma, V. Awana, A. Srivastava, T. Senguttuvan, S. Husale, *J. Phys.: Condens. Matter* **2017**, *29*, 115602.
[10] A. Fernández-Pacheco, L. Skoric, J. M. De Teresa, J. Pablo-Navarro, M. Huth, O. V. Dobrovolskiy, *Materials* **2020**, *13*, 3774.
[11] F. Xiu, L. He, Y. Wang, L. Cheng, L.-T. Chang, M. Lang, G. Huang, X. Kou, Y. Zhou, X. Jiang, Z. Chen, J. Zou, A. Shailos, K. L. Wang, *Nat. Nanotechnol.* **2011**, *6*, 216.
[12] S. S. Hong, W. Kundhikanjana, J. J. Cha, K. Lai, D. Kong, S. Meister, M. A. Kelly, Z.-X. Shen, Y. Cui, *Nano Lett.* **2010**, *10*, 3118.
[13] S. S. Hong, Y. Zhang, J. J. Cha, X.-L. Qi, Y. Cui, *Nano Lett.* **2014**, *14*, 2815.
[14] S. S. Hong, J. J. Cha, D. Kong, Y. Cui, *Nat. Commun.* **2012**, *3*, 757.
[15] A. F. Shevchun, G. K. Strukova, I. M. Shmyt'ko, G. V. Strukov, S. A. Vitkalov, D. S. Yakovlev, I. A. Nazhestkin, D. V. Shovkun, *Symmetry* **2022**, *14*, 2142.
[16] M. Rößler, D. Fan, F. Münning, H. F. Legg, A. Bliesener, G. Lippertz, A. Uday, R. Yazdanpanah, J. Feng, A. Taskin, Y. Ando, *Nano Lett.* **2023**, *23*, 2846.
[17] A. Cook, M. Franz, *Phys. Rev. B* **2011**, *84*, 201105.
[18] A. Cook, M. Vazifeh, M. Franz, *Phys. Rev. B* **2012**, *86*, 155431.
[19] M. Bai, X.-K. Wei, J. Feng, M. Luysberg, A. Bliesener, G. Lippertz, A. Uday, A. A. Taskin, J. Mayer, Y. Ando, *Commun. Mater.* **2022**, *3*, 20.
[20] M. Kayyalha, M. Kargarian, A. Kazakov, I. Miotkowski, V. M. Galitski, V. M. Yakovenko, L. P. Rokhinson, Y. P. Chen, *Phys. Rev. Lett.* **2019**, *122*, 047003.
[21] T. W. Schmitt, M. R. Connolly, M. Schleenvoigt, C. Liu, O. Kennedy, J. M. Chávez-Garcia, A. R. Jalil, B. Bennemann, S. Trellenkamp, F. Lentz, E. Neumann, T. Lindström, S. E. de Graaf, E. Berenschot, N. Tas, G. Mussler, K. D. Petersson, D. Grützmacher, P. Schüffelgen, *Nano Lett.* **2022**, *22*, 2595.
[22] R. V. Zakharov, O. V. Tikhonova, N. V. Klenov, I. I. Soloviev, V. N. Antonov, D. S. Yakovlev, *Adv. Quantum Technol.* **2024**, 2400141.
[23] T. W. Larsen, K. D. Petersson, F. Kuemmeth, T. S. Jespersen, P. Krogstrup, J. Nygård, C. M. Marcus, *Phys. Rev. Lett.* **2015**, *115*, 127001.
[24] J. Huo, Z. Xia, Z. Li, S. Zhang, Y. Wang, D. Pan, Q. Liu, Y. Liu, Z. Wang, Y. Gao, J. Zhao, T. Li, J. Ying, R. Shang, H. Zhang, *Chin. Phys. Lett.* **2023**, *40*, 047302.
[25] P. Schuffelgen, D. Rosenbach, C. Li, T. W. Schmitt, M. Schleenvoigt, A. R. Jalil, S. Schmitt, J. Kolzer, M. Wang, B. Bennemann, U. Parlak, L. Kibkalo, S. Trellenkamp, T. Grap, D. Meertens, M. Luysberg, G. Mussler, E. Berenschot, N. Tas, A. A. Golubov, A. Brinkman, T. Schäpers, D. Grützmacher, *Nat. Nanotechnol.* **2019**, *14*, 825.
[26] J. Kolzer, D. Rosenbach, C. Weyrich, T. W. Schmitt, M. Schleenvoigt, A. R. Jalil, P. Schuffelgen, G. Mussler, V. E. Sacksteder IV, D. Grutzmacher, H. Lüth, T. Schäpers, *Nanotechnology* **2020**, *31*, 325001.
[27] Y. S. Kim, M. Brahlek, N. Bansal, E. Edrey, G. A. Kapilevich, K. Iida, M. Tanimura, Y. Horibe, S.-W. Cheong, S. Oh, *Phys. Rev. B* **2011**, *84*, 073109.
[28] R. B. Jacobs-Gedrim, C. A. Durcan, N. Jain, B. Yu, *Appl. Phys. Lett.* **2012**, *101*, 143103.
[29] D. Belotcerkovtceva, J. Panda, M. Ramu, T. Sarkar, U. Noumbe, M. V. Kamalakar, *Nano Res.* **2023**, *16*, 4233.
[30] G. Kunakova, E. Kauranens, K. Niherysh, M. Bechelany, K. Smits, G. Mozolevskis, T. Bauch, F. Lombardi, D. Erts, *Nanomaterials* **2022**, *12*, 768.
[31] P. Schonherr, L. J. Collins-McIntyre, S. Zhang, P. Kusch, S. Reich, T. Giles, D. Daisenberger, D. Prabhakaran, T. Hesjedal, *Nanoscale Res. Lett.* **2014**, *9*, 1.
[32] D. S. Yakovlev, D. S. Lvov, O. V. Emelyanova, P. S. Dzhumaev, I. V. Shchetinin, O. V. Skryabina, S. V. Egorov, V. V. Ryazanov, A. A. Golubov, D. Roditchev, V. S. Stolyarov, *J. Phys. Chem. Lett.* **2022**, *13*, 9221.
[33] S. Engels, A. Epping, C. Volk, S. Korte, B. Voigtlander, K. Watanabe, T. Taniguchi, S. Trellenkamp, C. Stampfer, *Appl. Phys. Lett.* **2013**, *103*, 7.
[34] D. Bischoff, T. Krahenmann, S. Droscher, M. A. Gruner, C. Barraud, T. Ihn, K. Ensslin, *Appl. Phys. Lett.* **2012**, *101*, 20.
[35] L. A. Ponomarenko, F. Schedin, M. I. Katsnelson, R. Yang, E. W. Hill, K. S. Novoselov, A. K. Geim, *Science* **2008**, *320*, 356.
[36] A. Kurzmann, H. Overweg, M. Eich, A. Pally, P. Rickhaus, R. Pisoni, Y. Lee, K. Watanabe, T. Taniguchi, T. Ihn, K. Ensslin, *Nano Lett.* **2019**, *19*, 5216.
[37] X.-X. Song, D. Liu, V. Mosallanejad, J. You, T.-Y. Han, D.-T. Chen, H.-O. Li, G. Cao, M. Xiao, G.-C. Guo, G.-P. Guo, *Nanoscale* **2015**, *7*, 16867.
[38] A. Shilov, L. Elesin, A. Grebenko, V. Kleshch, M. Kashchenko, I. Mazurenko, E. Titova, E. Zharkova, D. Yakovlev, K. Novoselov, D. A. Ghazaryan, V. Dremov, D. A. Bandurin, *arXiv preprint arXiv:2406.16354* **2024**.
[39] A. Temiryazev, *Diamond Relat. Mater.* **2014**, *48*, 60.
[40] A. G. Temiryazev, M. Temiryazeva, A. V. Zdoroveyshchev, O. V. Vikhrova, Y. V. Nikulin, Y. V. Khivintsev, S. A. Nikitov, *Tech. Phys.* **2019**, *64*, 1716.
[41] B. Rasche, J. Brunner, T. Schramm, M. P. Ghimire, U. Nitzsche, B. Buchner, R. Giraud, M. Richter, J. Dufouleur, *Nano Lett.* **2022**, *22*, 3550.
[42] A. Levin, G. Gusev, A. Yaroshevich, Z. Kvon, A. Bakarov, *Phys. Rev. B* **2023**, *108*, 115310.
[43] S. V. Lutsenko, M. A. Kozhaev, O. V. Borovkova, A. N. Kalish, A. G. Temiryazev, S. A. Dagesyan, V. N. Berzhansky, A. N. Shaposhnikov, A. N. Kuzmichev, V. I. Belotelov, *Opt. Lett.* **2021**, *46*, 4148.
[44] M. A. Islam, P. Serles, B. Kumral, P. G. Demingos, T. Qureshi, A. Meiyazhagan, A. B. Puthirath, M. S. B. Abdullah, S. R. Faysal, P. M. Ajayan, D. Panesar, C. V. Singh, T. Filleter, *Appl. Phys. Rev.* **2022**, *9*, 4.
[45] V. Kumar, A. Kumar, D.-J. Lee, S.-S. Park, *Materials* **2021**, *14*, 4590.
[46] F. Campana, H. Buqa, P. Novák, R. Kötz, H. Siegenthaler, *Electrochem. Commun.* **2008**, *10*, 1590.
[47] D. F. Carrasco, S. Garcia-Dali, S. Villar-Rodil, J. M. Munuera, E. Raymundo-Pinero, J. I. Paredes, *ACS Appl. Energy Mater.* **2023**.
[48] B. L. Chauhan, S. A. Bhakhar, P. M. Pataniya, S. U. Gupta, G. Solanki, V. Pathak, V. Patel, *J. Mater. Sci.: Mater. Electron.* **2022**, *33*, 10314.
[49] X. Wang, L. You, D. Liu, C. Lin, X. Xie, M. Jiang, *Phys. C: Supercond.* **2012**, *474*, 13.
[50] Z. Velluire Pellat, E. Maréchal, N. Moulonguet, G. Saïz, G. Ménard, S. Kozlov, F. Couëdo, P. Amari, C. Medous, J. Paris, R. Hostein,

J. Lesueur, C. Feuillet-Palma, N. Bergeal, *Sci. Rep.* **2023**, *13*, 14366.
[51] E. Zimmermann, J. Kölzer, M. Schleenvoigt, D. Rosenbach, G. Mussler, P. Schüffelgen, T. Heider, L. Plucinski, J. Schubert, H. Lüth, D. Grützmacher, T. Schäpers, *Semicond. Sci. Technol.* **2023**, *38*, 035010.
[52] D. Mallick, S. Mandal, R. Ganesan, P. Anil Kumar, *Appl. Phys. Lett.* **2021**, *119*, 1.
[53] W. Wang, S. Hu, Q. Xie, *AIP Adv.* **2023**, *13*, 12.
[54] D. Khudaiberdiev, Z. D. Kvon, M. V. Entin, D. A. Kozlov, N. N. Mikhailov, M. Ryzhkov, *Nanomaterials* **2023**, *13*, 2882.
[55] R. Somphonsane, H. Ramamoorthy, G. He, J. Nathawat, S. Yin, C.-P. Kwan, N. Arabchigavkani, B. Barut, M. Zhao, Z. Jin, J. Fransson, J. P. Bird, *Sci. Rep.* **2020**, *10*, 5611.
[56] G. M. Gusev, Z. Kvon, E. Olshanetsky, A. Levin, Y. Krupko, J. Portal, N. Mikhailov, S. Dvoretsky, *Phys. Rev. B* **2014**, *89*, 125305.
[57] A. N. Obraztsov, P. G. Kopylov, B. A. Loginov, M. A. Dolganov, R. R. Ismagilov, N. V. Savenko, *Rev. Sci. Instrum.* **2010**, *81*, 1.
[58] M. Liu, J. Zhang, C.-Z. Chang, Z. Zhang, X. Feng, K. Li, K. He, L.-l. Wang, X. Chen, X. Dai, Z. Fang, Q.-K. Xue, X. Ma, Y. Wang, *Phys. Rev. Lett.* **2012**, *108*, 036805.
[59] D. Mo, W. Wang, Q. Cai, *Nanoscale Res. Lett.* **2016**, *11*, 1.
[60] Y. C. Arango, L. Huang, C. Chen, J. Avila, M. C. Asensio, D. Grützmacher, H. Lüth, J. G. Lu, T. Schäpers, *Sci. Rep.* **2016**, *6*, 29493.
[61] J. Zhang, P.-L. Tse, A.-R. Jalil, J. Kölzer, D. Rosenbach, M. Luysberg, G. Panaitov, H. Lüth, Z. Hu, D. Grützmacher, J. G. Lu, T. Schäpers, *Nat. Commun.* **2021**, *12*, 754.
[62] G. Seelig, S. Pilgram, A. N. Jordan, M. Büttiker, *Phys. Rev. B* **2003**, *68*, 161310.
[63] K.-T. Lin, Y. Lin, C. Chi, J. Chen, T. Ueda, S. Komiyama, *Phys. Rev. B: Condens. Matter Mater. Phys.* **2010**, *81*, 035312.
[64] Y. Ando, *J. Phys. Soc. Jpn.* **2013**, *82*, 102001.
[65] S. Hikami, A. I. Larkin, Y. Nagaoka, *Progr. Theoret. Phys.* **1980**, *63*, 707.
[66] A. Taskin, S. Sasaki, K. Segawa, Y. Ando, *Phys. Rev. Lett.* **2012**, *109*, 066803.
[67] N. Bansal, Y. S. Kim, M. Brahlek, E. Edrey, S. Oh, *Phys. Rev. Lett.* **2012**, *109*, 116804.
[68] B. Hamdou, J. Gooth, A. Dorn, E. Pippel, K. Nielsch, *Appl. Phys. Lett.* **2013**, *102*, 22.
[69] J. Chen, X. He, K. Wu, Z. Ji, L. Lu, J. Shi, J. Smet, Y. Li, *Phys. Rev. B* **2011**, *83*, 241304.
[70] H. Steinberg, J.-B. Laloë, V. Fatemi, J. S. Moodera, P. Jarillo-Herrero, *Phys. Rev. B* **2011**, *84*, 233101.
[71] L. Ohnoutek, M. Hakl, M. Veis, B. A. Piot, C. Faugeras, G. Martinez, M. V. Yakushev, R. W. Martin, C. Drav sar, A. Materna, G. Strzelecka, A. Hruban, M. Potemski, M. Orlita, *Sci. Rep.* **2016**, *6*, 19087.
[72] A. Frolov, A. Orlov, D. Voropaev, A. Hadj-Azzem, A. Sinchenko, P. Monceau, *Appl. Phys. Lett.* **2021**, *118*, 25.
[73] P. Kopylov, B. Loginov, R. Ismagilov, A. Obraztsov, *Instrum. Exp. Tech.* **2010**, *53*, 613.
[74] V. S. Stolyarov, D. Roditchev, V. L. Gurtovoi, S. N. Kozlov, D. S. Yakovlev, O. V. Skryabina, V. M. Vinokur, A. A. Golubov, *Adv. Quantum Technol.* **2022**, *5*, 2100124.
[75] D. S. Yakovlev, I. A. Nazhestkin, N. G. Ismailov, S. V. Egorov, V. N. Antonov, V. L. Gurtovoi, *Symmetry* **2023**, *15*, 550.